J Mater Sci
DOI 10.1007/s10853-014-8151-1

Biodegradable starch-based composites: effect of micro and nanoreinforcements on composite properties

Samaneh Karimi · Alain Dufresne · Paridah Md. Tahir · Ali Karimi · Ali Abdulkhani

Received: 6 November 2013 / Accepted: 7 March 2014

Abstract Thermoplastic starch (TPS) matrix was reinforced with various kenaf bast cellulose nanofiber loadings (0–10 wt%). Thin films were prepared by casting and evaporating the mixture of aqueous suspension of nanofibers (NFs), starch, and glycerol which underwent gelatinization process at the same time. Moreover, raw fibers (RFs) reinforced TPS films were prepared with the same contents and conditions. The effects of filler type and loading on different characteristics of prepared materials were studied using transmission and scanning electron microscopies, X-ray diffractometry, Fourier transform infrared spectroscopy, thermogravimetric analysis, differential scanning calorimetry, and moisture absorption analysis. Obtained results showed a homogeneous dispersion of NFs within the TPS matrix and strong association between the filler and matrix. Moreover, addition of nanoreinforcements decreased the moisture sensitivity of the TPS film significantly. About 20 % decrease in moisture content at equilibrium was observed with addition of 10 wt% NFs while this value was only 5.7 % for the respective RFs reinforced film.

S. Karimi (✉) · P. Md. Tahir · A. Karimi
Laboratory of Biocomposite Technology, Institute of Tropical Forestry and Forest Products (INTROP), University Putra Malaysia, 43400 Serdang, Selangor, Malaysia
e-mail: samanehkarimi82@gmail.com

A. Dufresne
Grenoble Institute of Technology, The International School of Paper, Print Media and Biomaterials (PAGORA), CS10065, 38402, Saint Martin d'Hères Cedex, France

A. Karimi · A. Abdulkhani
Department of Wood and Paper Science and Technology, Faculty of Natural Resources, University of Tehran, P.O. Box 31585-43114, Karaj, Iran

Introduction

Global ecological and environmental challenges create the necessity to replace petroleum-based materials by renewable resources. Nature is the source of a wide range of biomacromolecules that can be used in the preparation of green materials. Within this context, polysaccharides are the most abundant biopolymers on Earth, with cellulose, chitin, and starch dominating [1].

Starch can be found in various parts of a plant and is deposited in the form of semi-crystalline granules which are insoluble in cold water [1]. It has been estimated that total starch production from major starch crops will be 81.3 million tons by 2015 [2]. Starch can be easily processed to a natural and biodegradable polymeric matrix. The thermoplastic starch (TPS) was patented by the Warner-Lambert Company in 1992 [3] and was introduced as a starch that had been heated to a high enough temperature and for enough time. Under these conditions, the starch granules are melted and plasticized, forming a material that represent a thermoplastic behavior [1]. However, the problems associated with TPS films are high water sensitivity and weak mechanical properties which are highly affected by the relative humidity [4]. To address these issues, TPS can be reinforced by natural fibers.

Natural fibers are produced in billions of tons yearly around the world and are therefore abundant, inexpensive, and readily available. Their unique nanocellulosic structure can be isolated by a top-down approach and incorporated into polymeric matrices by a bottom-up approach to produce multi-functional, value-added materials that are sustainable, renewable, recyclable, and environmentally friendly.

The application of nanocelluloses isolated from natural fibers, as reinforcements in starch-based composites has

Published online: 03 April 2014

been studied in different works. For instance, nanocellulose isolated from bagasse [5], Cottonseed Linter [6], flax [7], hemp [8], wheat straw [9], and ramie [10] have been used to reinforce TPS matrix and great improvements in mechanical performance and water sensitivity have been reported.

Reviewing the published literature indicate that there is only one available work on kenaf nanocellulose-reinforced TPS [11]. In that research, acid hydrolyzed nanocrystallites from kenaf bast were incorporated into cassava glycerol/sorbitol plasticized starch matrix. It is important to highlight that nanocellulose used in this work was obtained by mechanical shearing so the morphology and surface chemistry of the used nanocellulose in this work is totally different from the mentioned work. Moreover very limited properties of nanocomposite films were discussed in that work [11]. In the present study, a broad range of composite properties is discussed.

Experimental

Nanofiber isolation

The preparation and characterization of cellulosic nanofibers from raw kenaf bast fibers were described elsewhere [12]. Water retted kenaf (*Hibiscus cannabinus* v36) bast fibers were kindly supplied by the Institute of Tropical Forestry and Forest Products (INTROP, UPM, Malaysia). Briefly, alkali treated fibers, without going through bleaching procedures, underwent mechanical shearing for nanocellulose isolation. The diameter range of isolated nanofibers was from 2.2 to 34 nm with the average value of 7 nm.

Film processing

Waxy maize starch is almost pure amylopectin (amylose content is lower than 1 %) and was kindly supplied by Cargill (Krefeld, Germany). Briefly, the starting products [starch + glycerol (98 % purity) + water + raw fibers (pulverized to 0.5 μm) or nanofiber suspension] were mixed and undergone the gelatinization process at the same time in order to obtain composite and nanocomposite films with a homogeneous dispersion. The glycerol content in the composition of all films was fixed at 33.33 wt% of total dry weight of materials while the fiber content varied from 0 to 10 wt%, and for each gram of starch 18.5 mg of distilled water was added.

Fabricated films were conditioned in a desiccator at 43 % relative humidity (RH) for 10 days at room temperature. Films were weighted regularly to ensure the equilibration of the moisture content in the films before various characterizations. Average formed film thickness was 0.4 mm.

Microscopy

The fractured surface of TPS and composite strips was examined using JEOL JSM-6400 and LEO 1455 VP scanning electron microscopes (SEM). Samples were cooled in liquid nitrogen, and then broken. The fractured surface was sputter coated with gold before viewing.

Transmission electron microscopy (TEM) images nanocomposite films were taken with a Hitachi TEM model H-7100. Samples were prepared by cryosectioning ultramicrotome.

Attenuated total reflectance Fourier transform infrared spectroscopy (ATR/FTIR)

Absorbance spectra of the matrix and composite samples were recorded on a Perkin-Elmer spectrometer 100 series using the attenuated total reflectance (ATR) accessories. Transmittance mode was recorded within the range of 4000–650 cm^{-1}.

X-ray diffraction (XRD)

X-ray diffraction measurements were conducted using X'pert Pro Panalytical PW 3040 MPD diffractometer. Patterns were recorded in the 2θ range of 4°–40°.

Thermal properties

Thermogravimetric analysis (TGA) was carried out with a TGA Q500 (TA Instruments) equipment. Data were obtained under linear temperature conditions. The temperature was swept from room temperature to 500 °C at a heating rate of 5 °C/min under a nitrogen atmosphere.

Differential scanning calorimetry (DSC) was performed with a DSC Q20 (TA Instruments) equipment, fitted with a nitrogen gas system. Tzero Aluminum hermetic pans were used. All the measurements were performed from room temperature to 250 °C at a heating rate of 10 °C/min. It is worth to note that for all DSC measurements an initial melting followed by a crystallization run were performed to remove thermal history of the samples.

Moisture uptake

The kinetics of moisture absorption was determined according to ASTM D 5229 at 98 % RH. The samples dimensions were 50 × 5 × 0.4 mm^3, therefore the film thickness (L) was considered thin enough for the molecular diffusion to be one-dimensional. The samples were dried at 100 °C overnight. After weighing, they were conditioned at room temperature in a desiccator of 98 % RH ($CuSO_4 \cdot 5H_2O$ saturated solution). The samples were removed at

specific intervals and were weighed until the equilibrium state was reached. Experiments were done in four replicates, and the average value was used. The moisture uptake (MU) of the samples was calculated according to Eq. (1):

$$\mathrm{WU}(\%) = \frac{M_t - M_0}{M_0} \times 100 \quad (1)$$

where M_0 and M_t are the weights of the sample before exposure to 98 % RH and after t h of exposure to 98 % RH, respectively.

The water diffusion coefficient (D) was also determined for an infinite slab with a constant D and at short times using Eq. (2) [13]:

$$\frac{M_t - M_0}{M_\infty} = \frac{4}{L}\left[\frac{Dt}{\pi}\right]^{\frac{1}{2}} \quad (2)$$

M_∞ is the equilibrium moisture sorption, and L is the thickness of the sample. The values of $(M_t - M_0)/M_\infty$ as a function of $t^{\frac{1}{2}}$ were plotted for all samples, and diffusion coefficients were calculated from the slope of initial linear part of these plots.

Results and discussion

Morphological characterization

Cryo-fractured surfaces of the neat matrix as well as composite and nanocomposite films were studied using SEM (Fig. 1).

For the TPS film, good interaction between the plasticizer and starch contributed to the continuous surface of the matrix (Fig. 1c). The images of fractured surfaces of the TPS-RF films (Fig. 1a, b) gave evidence of good interfacial adhesion as shown by the remaining starch on the surface of the pulled-out fibers [14, 15].

Regarding TPS-NF films, as compared to the neat film, the morphology of the NFs in the TPS-NF films can be easily identified in the texture of the fractured surfaces (Fig 1d–f). NFs appeared like white dots which concentration is a direct function of the filler content in the composite [16]. The homogeneous surface of TPS-NF films demonstrated good dispersion of NFs within the TPS matrix. No aggregates were visible in the micrographs indicating a proper interaction between NFs and TPS in the studied materials. This is attributed to the good compatibility resulting from the structural similarities between starch and cellulose and the possible hydrogen bonding interactions existing at the interface between filler and matrix [7].

TEM micrographs of the neat TPS and nanocomposite films are presented in Fig. 2. It can be seen that the nanofibers are embedded individually in the matrix and no apparent aggregation was observed.

Thermal properties

The thermogravimetric (TG) and derivative thermogravimetric (DTG) curves of all prepared films are shown in Fig. 3. Obtained data clearly showed that both TPS-RF and TPS-NF films were more thermally stable than the starch/glycerol matrix due to good interaction between fibers and the matrix phase [17]. In panels c and d of the figure, TG and DTG curves of the nanofiber and starch powder have been overlaid with the respective curves of the TPS and TPS-NF 2 %. As it can be seen from the curves, thermal stability of the nanocomposite film has been located in between its constituent materials.

It is well known that thermal decomposition of the starchy matrix occurs in three main steps [18, 19]. The same trend has been observed in this study. According to DTG curves, the initial peak corresponds to the vaporization of water and low-molecular-weight compounds [20]. The second peak is attributed to the decomposition of the glycerol-rich phase [15, 18]. The third peak (main peak) is due to the oxidation of the partially decomposed starch as well as fibers degradation.

The main degradation peak temperature of studied samples is shown in Table 1. According to this table, the T_{max} values of nanocomposite films shifted toward higher temperatures only until 8 wt% fiber content and could be due to the closer association of nanofiber network with glycerol. Another explanation could be the high content of the nanofibers that restricts the contact surface between the matrix and the filler.

Higher amount of residue in the reinforced films as opposed to the neat TPS film was observed. It is due to the presence of ash in fibers which have low degradation rate [21–23]. A bolder temperature shoulder around 250 °C can be observed in the DTG curve of TPS-RF films (Fig. 3f). This is attributed to the presence of hemicellulose [24] in raw fiber, and its refinement in the curves of TPS-NF films is due to hemicellulose removal during the applied treatments.

DSC analysis of TPS, TPS-RF, and TPS-NF samples showed that the melting occurs over a narrow temperature range (Fig. 4a, b). Generally, no significant effect on the melting point of composite films with reference to the unfilled matrix was observed. This finding is in agreement with Savadekar and Mhaske work [25]. In the case of TPS-NF 10 % film, a significant shift toward lower temperatures was observed, in agreement with its related TGA results. It

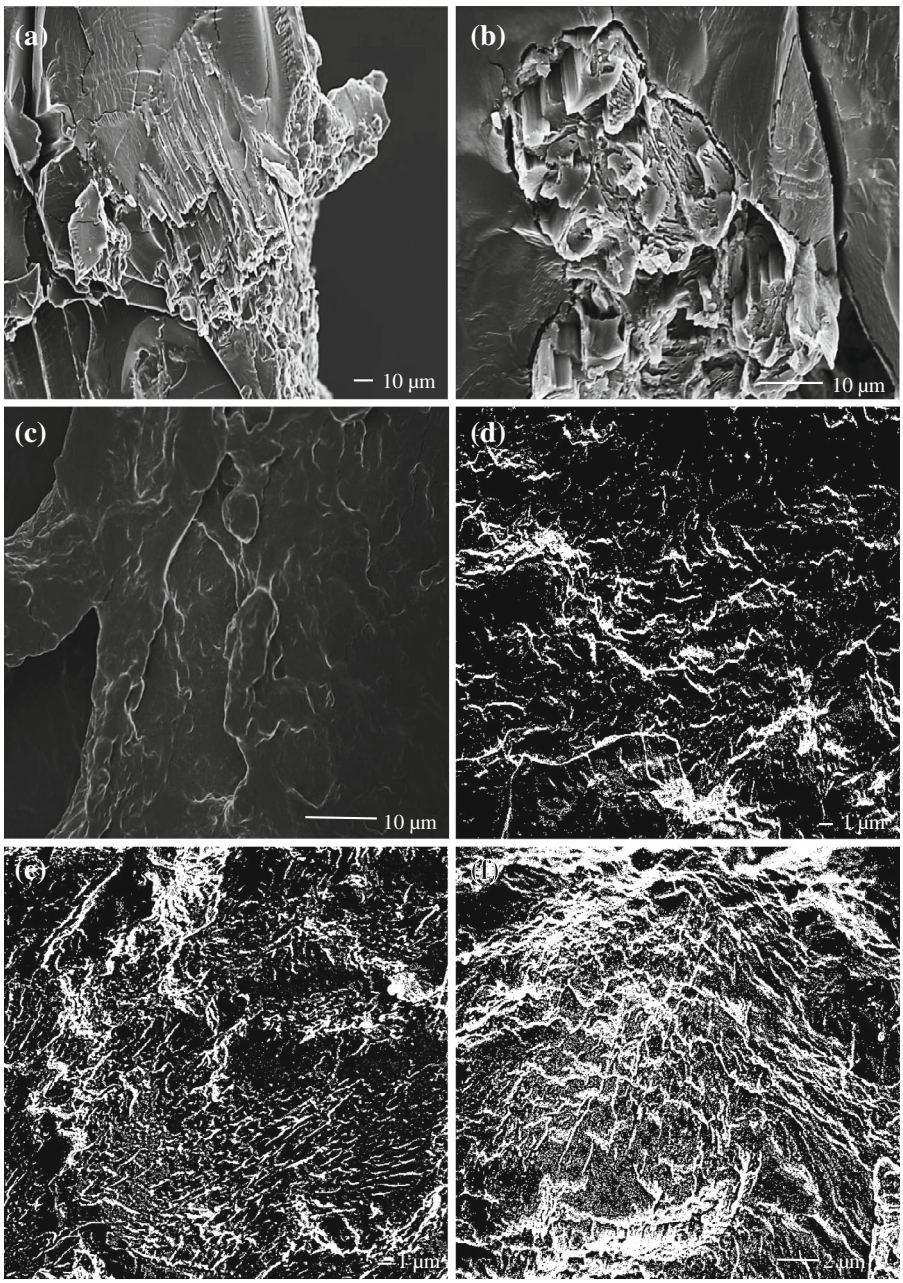

Fig. 1 SEM micrographs of: **a**, **b** TPS-RF 6 % **c** TPS **d** TPS-NF 6 % **e** TPS-NF 8 % **f** TPS-NF 10 %

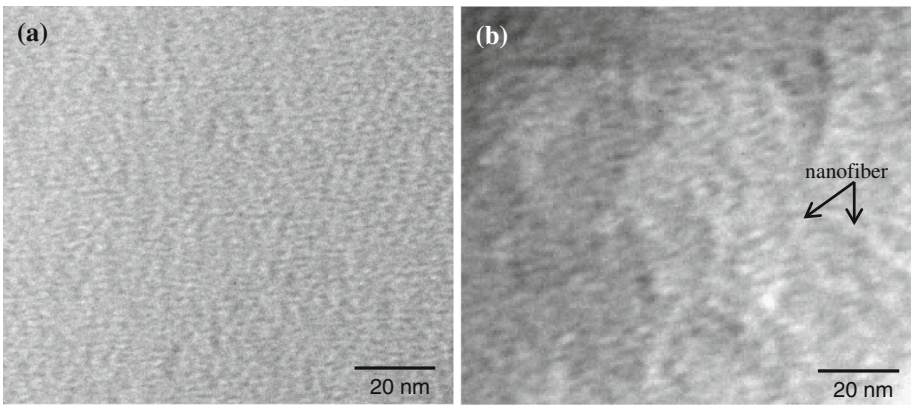

Fig. 2 TEM micrographs of **a** TPS film **b** nanocomposite film (TPS-NF 6 %)

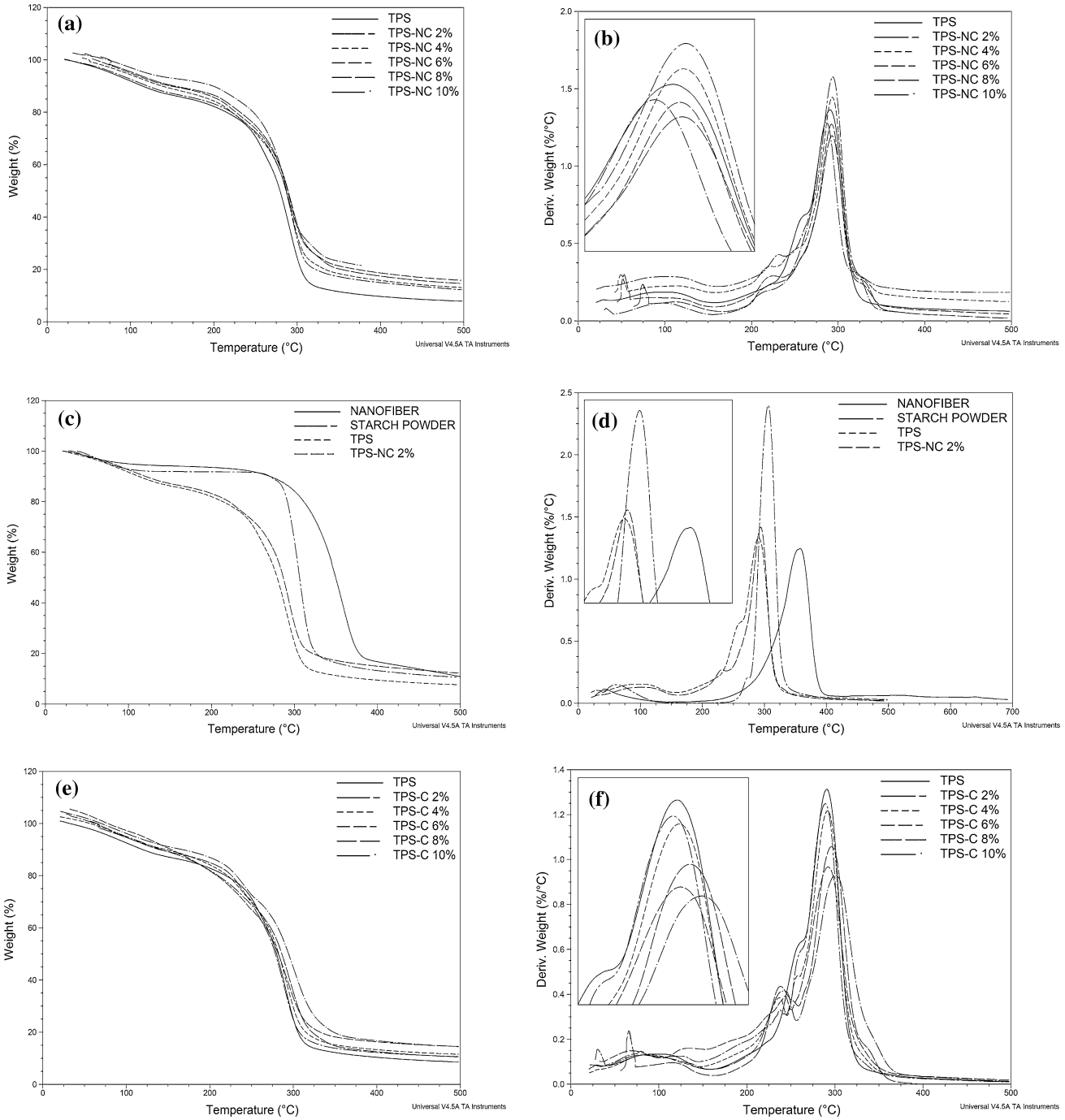

Fig. 3 TG (**a**, **c**, **e**) and DTG (**b**, **d**, **f**) curves of fabricated materials (Samples codes are indicated in the figures)

could be ascribed to a reduction of starch crystallite size. However, regarding TPS-RF films not such a specific trend was observed. The heat of fusion (ΔH_f) as calculated from the area under the peak for all samples (Table 1). As can be seen the ΔH_f values have been increased by increasing the fiber content in both types of composites. Moreover these values for the TPS-NF films are significantly higher than the TPS-RF counterparts. These results are representative of films crystallinity increment in accordance with fiber type and content.

Attenuated total reflectance Fourier transform infrared spectroscopy

The FTIR spectra of the TPS and TPS-NF films are depicted in panel a of Fig. 5, while the spectra of TPS-RF

Table 1 Recorded DTG peak temperature (from TGA data) and heat of fusion, values (from DSC data) of the studied materials

Fiber content (wt%)	TPS-NF		TPS-RF	
	DTG (°C)	ΔH_f (J/g)	DTG (°C)	ΔH_f (J/g)
0	289.9	61.5	289.9	61.5
2	293.6	134.2	289.9	67.1
4	294.1	134.8	291.5	109.4
6	295.4	136.0	291.9	117.3
8	296.7	143.1	295.9	118.2
10	286.7	161.2	296.6	128.3

10 % has been overlaid with obtained spectra of TPS-NF 10 % and the neat film (TPS) in panel b.

The overall characteristics of both constituent polymers, cellulose and TPS, could be found in the spectra. The neat TPS films as well as both types of composite films, regardless the fiber content, displayed almost similar features in the whole FTIR spectral range. This is due to the chemical similarities between starch and cellulose. Although the FTIR spectra of samples and matrix show only slight differences, they were repeated in all the tests made on different samples. Similar results had been previously reported [7, 26, 27].

The broad absorption band in the 3400–3200 cm^{-1} region is attributed to the –OH stretching vibration in cellulose and TPS. However, the transmittance intensity of stretching vibrations of –OH groups in the FTIR spectra of composite and nanocomposite films were weakened accordingly with rise in fiber content, indicating that hydrogen bonding between starch molecules was partially destroyed [7]. The peaks around 2900–2800 cm^{-1} are ascribed to the stretching of C–H [28]. The

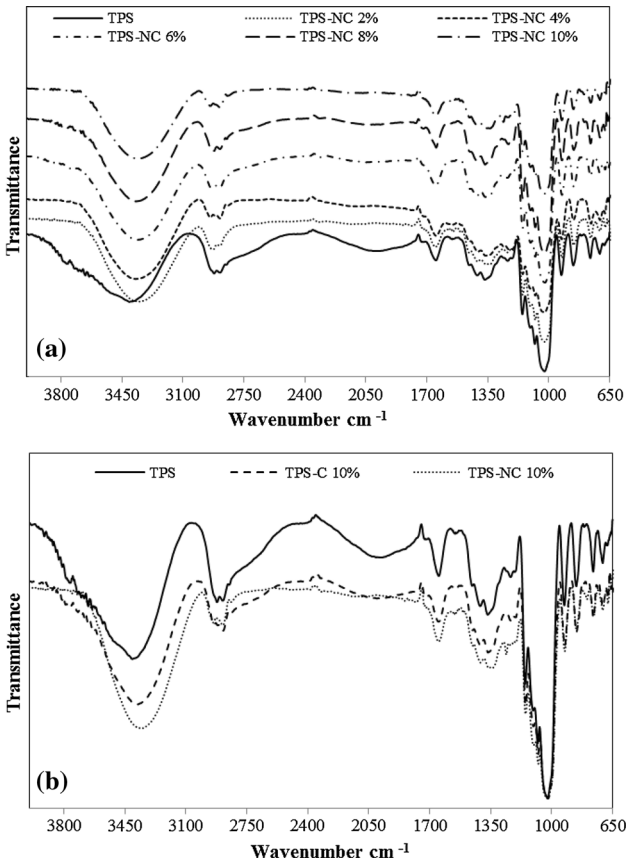

Fig. 5 FTIR spectra of fabricated materials (Samples codes are indicated in the figures)

1430–1431 cm^{-1} transmittances in the IR spectra of films are associated to the CH_2 symmetric bending [29]. The peaks around 1010–1070 cm^{-1} are due to the stretching of C–O and O–H groups and can be seen in the spectra of all materials. The peaks in the 1380–1320 cm^{-1} region are

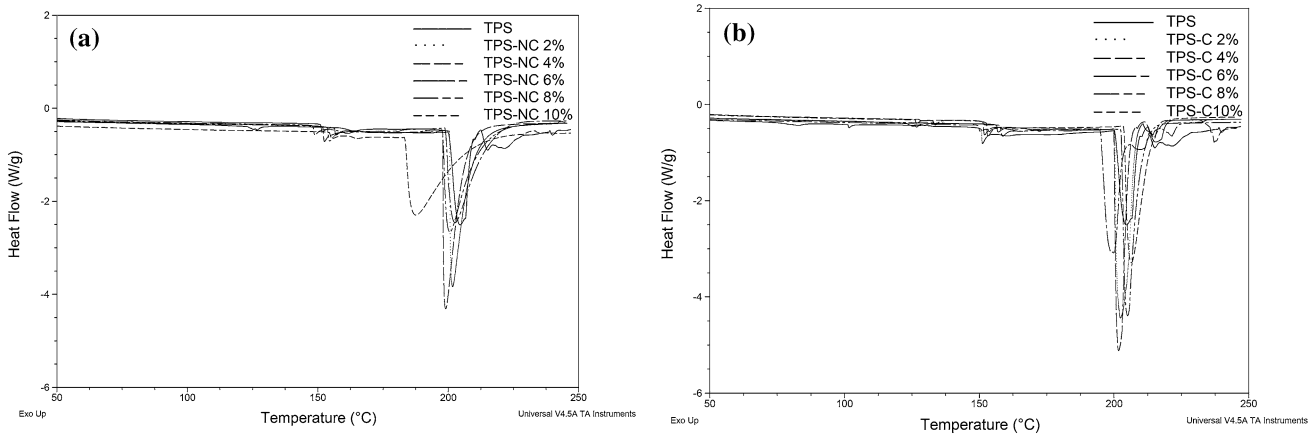

Fig. 4 DSC curves of fabricated materials (Samples codes are indicated in the figures)

also visible in the spectra of all materials and are ascribed to the bending vibration of C–H and C–O groups of the polysaccharides [29, 30]. The observed peaks in the 1650 and 1620 cm^{-1} region of the neat TPS and composite films are associated to the adsorbed water [29, 30]. The peak at 993 cm^{-1} in the spectra for all samples are attributed to the C–O stretching vibrations in starch [31]. Finally, the slight changes in the peak position with change in filler type and fiber content suggest new interactions between cellulose and starch molecules.

X-ray diffraction

The recorded XRD patterns for TPS and TPS-NF films are depicted in Fig. 6a, while Fig. 6b compared the XRD pattern of composite and nanocomposite films with 10 wt% fiber content. The crystalline order observed in the native starch granules is completely destroyed in TPS but, because of the mobility of the starch chains, recrystallization occurs, leading generally to the formation of B-, V-, and E-type crystalline structures [1].

For all studied materials major peaks were observed at $2\theta = 14.5°$, 16.8°, 20.5°, and 22.5°. These peaks are characteristic of cellulose type I from one side [16, 32] and the TPS from the other side [5, 33]. This observation showed that the diffractograms of composite films are only superimpositions of the diffractograms of the two components; starch and cellulose. With increasing the fiber content the magnitude of the peaks became more significant, especially in the case of TPS-NF films. This was clearly expected as the NFs are highly crystalline materials (CI 79.4 %). Therefore, increasing the NFs content increases the crystalline regions of the obtained composite film. This boost in the crystallinity of the medium leads to improvement of mechanical properties of the films accordingly.

Moisture uptake

Moisture sorption experiments data showed two well-defined zones in the sorption kinetic of all studied materials (Fig. 7). At the beginning of the experiment, $t < 10$ h, sorption kinetic was fast (zone I), meanwhile at extended times the kinetics of absorption stabilized and led to a plateau (zone II) which corresponds to the moisture uptake at equilibrium.

Moisture uptake of plasticized starch films was the highest, 63 %, compared to the composite films. Addition of raw fibers was effective in improving moisture resistance of TPS. This is mainly due to the constraining effect of the reinforcement to the material expansion as moisture is being absorbed [1]. Nanofiber-filled composites showed a significant leap in moisture resistance which could be attributed to the chemical structural similarity of nanocellulosic fibers and starch matrix. Reduction of moisture absorption of two hydrophilic materials, starch and cellulose, can be explained by the following factors: (1) good interfacial adhesion between cellulose and starch; (2) less hygroscopicity of cellulose regarding to starch; (3) formation of fibrous network around or between starch material which could hinder the moisture penetration [16]; and (4) high crystallinity of cellulose compared to starch.

Table 2 presented the values for moisture uptake at equilibrium and water diffusion coefficients (D) of TPS and TPS-NF films. Therefore, it can be concluded that the swelling of the material is suppressed in the presence of NFs within the TPS matrix. Similar results were previously reported [5, 6, 10, 16, 34]. The TPS film showed the highest D value, while with increasing fiber content from 0 to 10 wt%, this value decreased from 2.85×10^{-10} to 2.17×10^{-10} cm^2 s^{-1}. This is due to the formation of a 3D nanofibrillar network as well as strong hydrogen bonding between reinforcements and the TPS matrix.

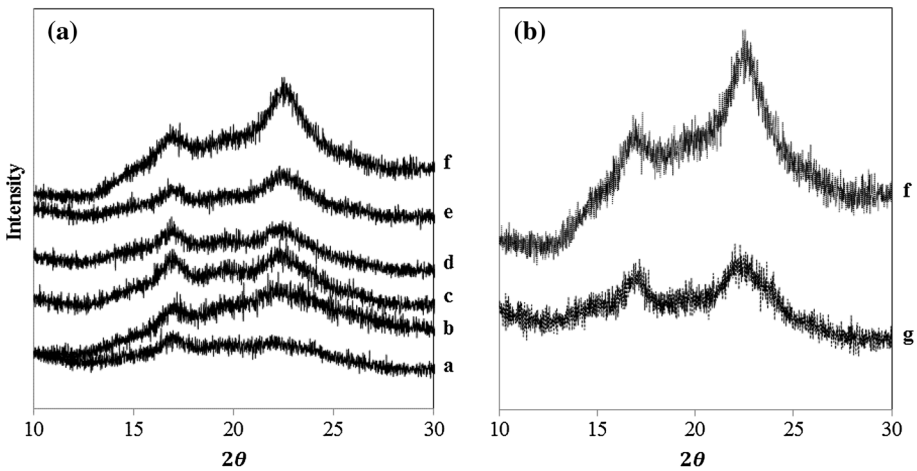

Fig. 6 XRD patterns of fabricated materials: **a** TPS **b** TPS-NF 2 % **c** TPS-NF 4 % **d** TPS-NF 6 % **e** TPS-NF 8 % **f** TPS-NF 10 % **g** TPS-RF 10 %

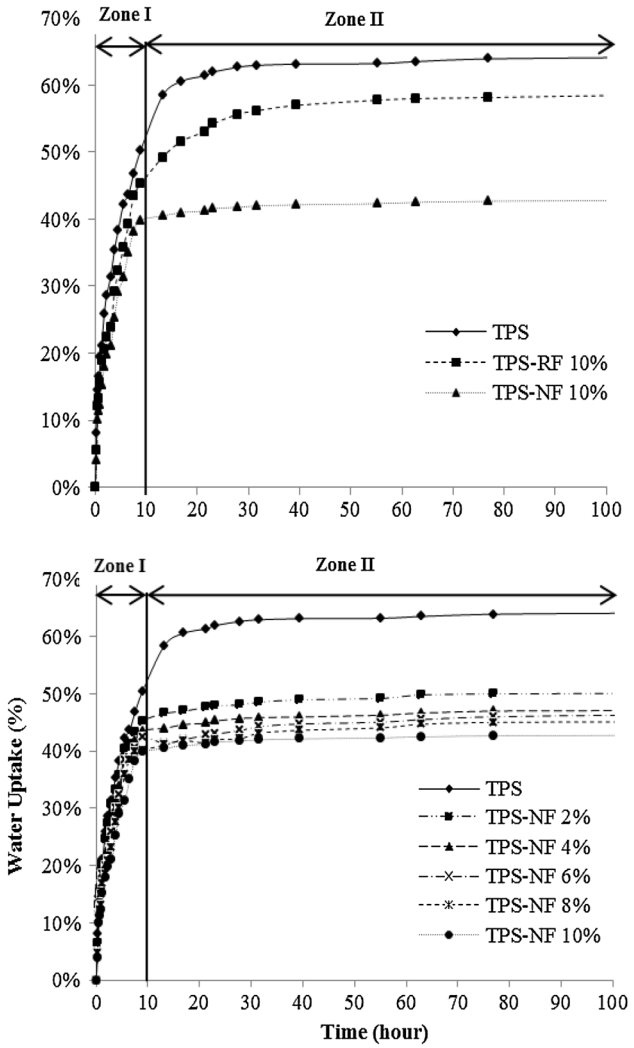

Fig. 7 Moisture uptake of the TPS film and biocomposites conditioned at 98 % RH as a function of time (Samples codes are indicated in the figures)

Table 2 Moisture content at equilibrium and water diffusion coefficient of materials conditioned at 98 % RH

Materials	Moisture content at equilibrium[a] (%)	Diffusion coefficient ($cm^2\ s^{-1} \times 10^{-10}$)
TPS	63.60[a]	2.85
TPS-RF 10 %	57.89[b]	2.69
TPS-NF 2 %	49.64[c]	2.61
TPS-NF 4 %	46.61[d]	2.57
TPS-NF6 %	45.54[e]	2.43
TPS-NF 8 %	44.52[e]	2.28
TPS-NF 10 %	42.50[f]	2.17

[a] Means that do not share a letter within the same column are significantly different at 2 % significance level based on the ANOVA and Tukey–Kramer pairwise comparison test

Conclusions

A cellulosic nanofibril suspension from kenaf bast was used to reinforce a TPS matrix with varying contents in the range of 0–10 wt% by a casting method. Raw fiber reinforced TPS films were processed under the same conditions to elucidate the effect of fiber dimension on the performance of materials. SEM and TEM micrographs of the cryo-fractured surface of materials displayed homogeneous dispersion of NFs within the TPS matrix, indicating strong association between matrix and nanofiller. XRD results revealed that the diffractograms of composite films are only superimpositions of the diffractograms of the two components; starch and cellulose, and with increasing the fiber content the magnitude of the XRD peaks became more significant. FTIR graphs of the fabricated materials displayed almost similar features in the whole spectral range, regardless the fiber content. TGA studies confirm that thermal decomposition of the starchy matrix occurs in three main steps, and the T_{max} values of composite films shifted toward higher temperatures. The TPS-NF 8 % film was the most thermally stable over all. According to DSC studies no significant effect on the melting point of composite films with reference to the unfilled matrix was observed. Moreover, addition of the nanoreinforcements decreased the moisture sensitivity of the TPS film significantly and 21 % decrease in moisture content at equilibrium was observed with addition of 10 wt% nanofiber.

Acknowledgements Authors would like to thank Mrs. Ashraf Zohrabi for her sincere assistance in preparing nanocomposite samples. Many thanks are expressed to Mr. Mehdi Hassani for his faithful support and help in editing the manuscript. The institute of tropical forestry and forest products (INTROP) is acknowledged for financial and technical support of the research.

References

1. Carvalho AJ (2008) Starch: major sources, properties and applications as thermoplastic materials. In: Mohamed Naceur Belgacem AG (ed) Monomers, polymers and composites from renewable resources. Elsevier, Amsterdam, pp 321–342
2. SK Patil (2009) Global modified starch derivatives markets a strategic review. http://www.marketresearch.com/S-K-Patil-and-Associates-v3203/Global-Modified-Starch-Derivatives-strategic-7083413/1-98
3. Lay G, Rehm J, Stepto RF et al (1992) Polymer compositions containing destructurized starch. US Patent 5,095,054. US Patent and Trademark Office, Washington, DC
4. Kumar AP, Singh RP (2008) Biocomposites of cellulose reinforced starch: improvement of properties by photo-induced crosslinking. Bioresour Technol 99:8803–8809
5. EdM Teixeira D, Pasquini AA Curvelo, Corradini E, Belgacem MN, Dufresne A (2009) Cassava bagasse cellulose nanofibrils reinforced thermoplastic cassava starch. Carbohydr Polym 78:422–431

6. Lu Y, Weng L, Cao X (2005) Biocomposites of plasticized starch reinforced with cellulose crystallites from cottonseed linter. Macromol Biosci 5:1101–1107
7. Cao X, Chen Y, Chang P, Muir A, Falk G (2008) Starch-based nanocomposites reinforced with flax cellulose nanocrystals. Express Polym Lett 2:502–510
8. Cao X, Chen Y, Chang PR, Stumborg M, Huneault MA (2008) Green composites reinforced with hemp nanocrystals in plasticized starch. J Appl Polym Sci 109:3804–3810
9. Kaushik A, Singh M, Verma G (2010) Green nanocomposites based on thermoplastic starch and steam exploded cellulose nanofibrils from wheat straw. Carbohydr Polym 82:337–345
10. Lu Y, Weng L, Cao X (2006) Morphological, thermal and mechanical properties of ramie crystallites—reinforced plasticized starch biocomposites. Carbohydr Polym 63:198–204
11. Zainuddin SYZ, Ahmad I, Kargarzadeh H, Abdullah I, Dufresne A (2012) Potential of using multiscale kenaf fibers as reinforcing filler in cassava starch-kenaf biocomposites. Carbohydr Polym 92:2299–2305
12. Karimi S, Tahir PM, Karimi A, Dufresne A, Abdulkhani A (2014) Kenaf bast cellulosic fibers hierarchy: a comprehensive approach from micro to nano. Carbohydr Polym 101:878–885
13. Vergnaud JM (1991) Liquid transport processes in polymeric materials: modeling and industrial applications. Prentice Hall, Englewood Cliffs
14. Soykeabkaew N, Laosat N, Ngaokla A, Yodsuwan N, Tunkasiri T (2012) Reinforcing potential of micro- and nano-sized fibers in the starch-based biocomposites. Compos Sci Technol 72:845–852
15. Martins IM, Magina SP, Oliveira L et al (2009) New biocomposites based on thermoplastic starch and bacterial cellulose. Compos Sci Technol 69:2163–2168
16. Angles MN, Dufresne A (2000) Plasticized starch/tunicin whiskers nanocomposites. 1. Structural analysis, Macromolecules 33:8344–8353
17. Chang PR, Jian R, Zheng P, Yu J, Ma X (2010) Preparation and properties of glycerol plasticized-starch (GPS)/cellulose nanoparticle (CN) composites. Carbohydr Polym 79:301–305
18. García NL, Ribba L, Dufresne A, Aranguren M, Goyanes S (2011) Effect of glycerol on the morphology of nanocomposites made from thermoplastic starch and starch nanocrystals. Carbohydr Polym 84:203–210
19. Jiang W, Qiao X, Sun K (2006) Mechanical and thermal properties of thermoplastic acetylated starch/poly (ethylene-co-vinyl alcohol) blends. Carbohydr Polym 65:139–143
20. Cyras VP, Tolosa Zenklusen MC, Vazquez A (2006) Relationship between structure and properties of modified potato starch biodegradable films. J Appl Polym Sci 101:4313–4319
21. Ashori A, Harun J, Raverty WD, Yusoff MNM (2006) Chemical and morphological characteristics of Malaysian cultivated kenaf (*Hibiscus cannabinus*) fiber. Polym Plast Technol Eng 45: 131–134
22. Yang H, Yan R, Chen H, Lee DH, Zheng C (2007) Characteristics of hemicellulose, cellulose and lignin pyrolysis. Fuel 86:1781–1788
23. Jonoobi M, Harun J, Shakeri A, Misra M, Oksman K (2009) Chemical composition, crystallinity, and thermal degradation of bleached and unbleached kenaf bast (*Hibiscus cannabinus*) pulp and nanofibers. BioResources 4:626–639
24. Rosa MF, Medeiros ES, Malmonge JA et al (2010) Cellulose nanowhiskers from coconut husk fibers: effect of preparation conditions on their thermal and morphological behavior. Carbohydr Polym 81:83–92
25. Savadekar N, Mhaske S (2012) Synthesis of nano cellulose fibers and effect on thermoplastics starch based films. Carbohydr Polym 89:146–151
26. Chen Y, Cao X, Chang PR, Huneault MA (2008) Comparative study on the films of poly (vinyl alcohol)/pea starch nanocrystals and poly (vinyl alcohol)/native pea starch. Carbohydr Polym 73:8–17
27. García NL, Ribba L, Dufresne A, Aranguren MI, Goyanes S (2009) Physico-mechanical properties of biodegradable starch nanocomposites. Macromol Mater Eng 294:169–177
28. Khalil H, Ismail H, Rozman H, Ahmad M (2001) The effect of acetylation on interfacial shear strength between plant fibres and various matrices. Eur Polymer J 37:1037–1045
29. Le Troedec M, Sedan D, Peyratout C et al (2008) Influence of various chemical treatments on the composition and structure of hemp fibres. Compos A 39:514–522
30. Nacos M, Katapodis P, Pappas C et al (2006) Kenaf xylan–a source of biologically active acidic oligosaccharides. Carbohydr Polym 66:126–134
31. Zhang Y, Han J (2006) Plasticization of pea starch films with monosaccharides and polyols. J Food Sci 71:253–261
32. Klemm D, Heublein B, Fink HP, Bohn A (2005) Cellulose: fascinating biopolymer and sustainable raw material. Angew Chem Int Ed 44:3358–3393
33. Rindlava Å, Hulleman SH, Gatenholma P (1997) Formation of starch films with varying crystallinity. Carbohydr Polym 34:25–30
34. Dufresne A, Dupeyre D, Vignon MR (2000) Cellulose microfibrils from potato tuber cells: processing and characterization of starch–cellulose microfibril composites. J Appl Polym Sci 76: 2080–2092